Journal of Fundamental and Applied Sciences

Research Article

ISSN 1112-9867

Available online at http://www.jfas.info

ELECTROCHEMICAL BEHAVIOR OF ZINC ANODE IN ACIDIC ZINC ELECTROLYTE - INFLUENCE OF LEAD AS AN IMPURITY IN ZINC ANODIC DISSOLUTION

Habiba Kherrab-Boukezzata[1,2*], Naima Ghemmit-Doulache[1,2], Moussa Bounoughaz[2], Slimane Boutarfaia[3]

[1]Université M'hamed Bougara de Boumerdes, Faculty of Science, Chemistry Department,

[2]Université M'hamed Bougara de Boumerdes, Fibrous Polymers Treatment and Forming Laboratory, Faculty of Technology, Avenue of Independence-35000-Algeria

[3]Laboratory of Metallurgy, Centre de Recherche Nucleaire Draria Alger-Algeria

Received: 14 June 2021 / Accepted: 21 April 2022 / Published: 26 April 2022

ABSTRACT

Zinc is common metal used for steel protection. In this work, an alloy Zn-1 % wt. Pb was prepared by fusion at 500°C. The analysis of the corrosion behavior was studied with pure Zn anode as control in aerated solution of 0.9 M $ZnSO_4.7H_2O$ + 1.63 M H_2SO_4 at 38°C.The effect of lead impurity on corrosion resistance of zinc anode in zinc electrorefining process was investigated using open circuit potential (OCP), Tafel plots, chronoamperometry at imposed constant anodic potential and electrochemical impedance spectroscopy (EIS) techniques. Samples were characterized by chemical analysis, optic microscope (OM) and X-ray diffraction (XRD). The results show that the lead impurity leads to degradation of the behavior of the alloy due to negative effect on the microstructure. Lead increases the corrosion rate and decreases the corrosion resistance of Zn-1 % wt. Pb alloy.

Keywords: Zinc electrorefining process, impurity, pure Zn and Zn-1 % wt. Pb anodes, acidic solution, microstructure, anodic corrosion behavior.

Author Correspondence, e-mail: n.ghemmit@univ-boumerdes.dz

doi: http://dx.doi.org/10.4314/jfas.1142

1. INTRODUCTION

Zinc (Zn) is one of the most important non-ferrous metals in national economic development in Algeria with ALZINC society production capacity of 36850 tones/year in 2012 [1]. This metal is produced from its ores of sulfide, oxide and siliceous types via pyro-electrometallurgical route. 85-90% of the world's zinc are produced by hydro-electrometallurgical routes [2-4] and from zinc sulphate electrolyte refining [5,6]. Zn obtained by this route still contains a quantity of impurity of about 1% of lead. Zinc is globally the fourth most widely used metal after iron, aluminum and copper [7-11]. Today its annual production is worldwide approximately 13 million tones per year and it is expected to continue growing at 2-3% per year [10,12]. Electrorefining is one of the commonly practiced industrial process compared to electrowinning for the final recovery of zinc at 99.999%. Zinc consumption is classified as follows: 50% for steel galvanisation, 17% as alloying element in cast alloys, 17% in cast alloys of brass and bronze and 16% in chemicals [9,10,13]. For this reason, the zinc corrosion and electrochemistry has been studied extensively in the literatures [9,14]. In addition, zinc is an important component in building materials, paints, cosmetics, medicine, pharmaceuticals, energy storage batteries, electrical equipment, automotive and textile industry and other industries [14-17]. Zinc is very important for human health [12,16]. Zinc metal is widely used for casting industries because of its low melting point and excellent fluidity. The zinc dross consists mainly of zinc metal (as high as 95 %). This dross can be directly melted into impure anodes and electro-refined to produce high purity zinc (99.999 %) through electrolysis [18]. Electrorefining is an electrolytic process. In which direct current is applied and zinc ions dissolve from the impure zinc anode to the electrolyte before its deposition onto the zinc cathode. The best anode must meet the following characteristics as high conductivity, excellent activity, good mechanical intensity, anticorrosive properties in aggressive sulfate environments [19] and in highly concentrated H_2SO_4 at high temperature [20], because the rate dissolution of anodes is the main source of contamination to the final zinc product. The relatively short service time of the anode material is one of the factors that lead to the increasing production cost of pure zinc by electro-refining [20], nowadays, zinc sulfate baths were considered as alternative due to their low cost and eco-friendliness [21]. Usually, sulphuric acid is used as

leaching medium for the dissolution of zinc [15,22]. The anode impurities such as Pb, Si, Cu, Fe, Ni, S accelerate the passivation by slime forming and are removed. These impurities can either deteriorate or improve the anodic performance [23] and are involved either as an insoluble residue based on nobler metals than zinc and insoluble components which will not dissolve anodically and they will be collected as anode sludge (anode slime) or soluble ignoble species which are dissolved into the electrolyte [24,25]. Therefor impurities can be a primary source of surface roughness and can affect the physiochemical properties of the electrolyte and the deposit quality of zinc in the cathode. Pb is nobler than Zn and therefore will not dissolve anodically and remain in the anode slime, that contains a significant amount of zinc powder. The floating slime cause irregular growth on the cathode. When the sludge becomes thick and non-porous, the active surface of the anode and the electrolysis current decrease and we have passivation. Passivation is the inhibition of dissolution reaction caused by formation of non-dissolving films, usually $ZnSO_4$. x H_2O. This passivation causes real problems during the zinc electrorefining. An excessive current density increases impurity levels in the cathode deposit. For the moment, refiners are trying to use low current densities imposed to the anodes to avoid rapid passivation and entrainment of the suspended particles towards the cathode, thus resulting in 99.999 % pure cathodic zinc.

The main aim of this study is to investigate the dissolution process of the zinc anode in sulfate system and to study experimentally, the effect of lead as impurity on the anodic dissolution process and on the slime formation during the zinc electro-refining.

2. RESULTS AND DISCUSSION

2.1. Analysis per fluorescence X

The chemical composition of pure zinc used in this study is given in table 1.

Table 1. Chemical composition of pure zinc

Chemical element	**Cr**	**Mn**	**Co**	**V**	**P**	**Ti**	**Al**	**Mo**	**Nb**
%	<0.001	<0.001	<0.001	<0.001	<0.001	<0.001	<0.001	<0.001	<0.001
Chemical element %	**S**	**Ni**	**Fe**	**Cu**	**Si**	**Ca**	**Mg**	**Zn**	
	0.012	0.013	0.016	0.029	0.140	Trace	Trace	99.790	

The result of this analysis is purely semi-quantitative. The zinc value given in the table 1 was calculated by difference.

2.2. Characterization of the surface samples

The XRD patterns of pure Zn and Zn-1 % wt. Pb alloy are shown in the figure 1.

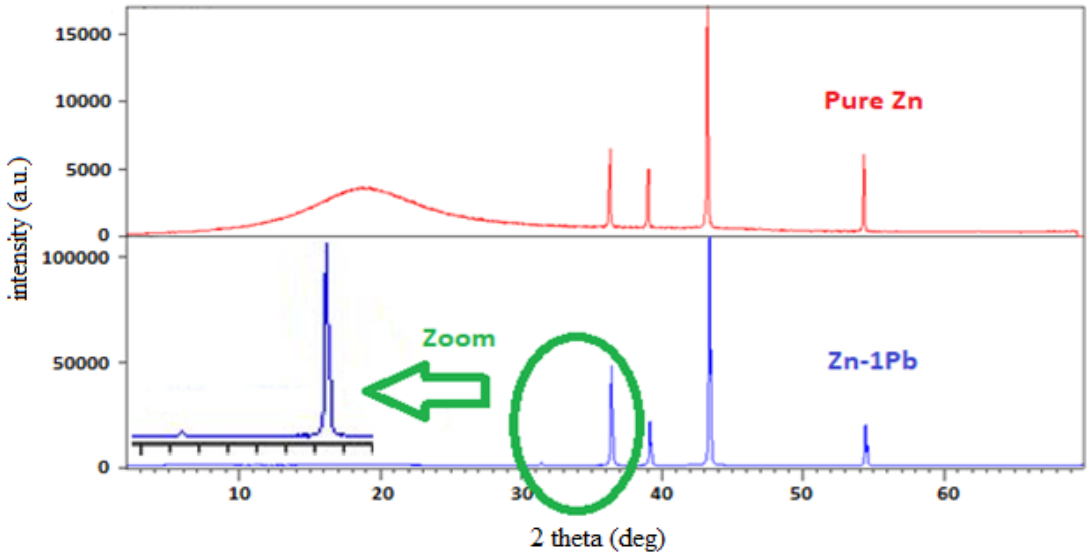

Fig.1. XRD patterns of pure zinc and zinc-1 % wt. lead alloy

For pure Zn, only the peaks original from Zn matrix at 2Θ position of 36.29°, 38.994°, 43.221°, 54.321° are detected [26-34]. For Zn-1 % wt. Pb, a small single peak at 2Θ position of 31.306° is identified, its low intensity is due to the low percentage of lead [35-37].

The OM micrographs (Figure 2) of the surface of the samples of pure zinc and the Zn-1 % wt. Pb alloy, having undergone mechanical polishing followed by chemical attack in a solution of (5 ml HNO_3 in 100 ml of deionised water for 5 seconds), show that the microstructure of this

material is composed of a first zinc-rich phase (η-Zn, compact hexagonal) and a second Pb- rich phase (α-Pb, face-centred cubic).

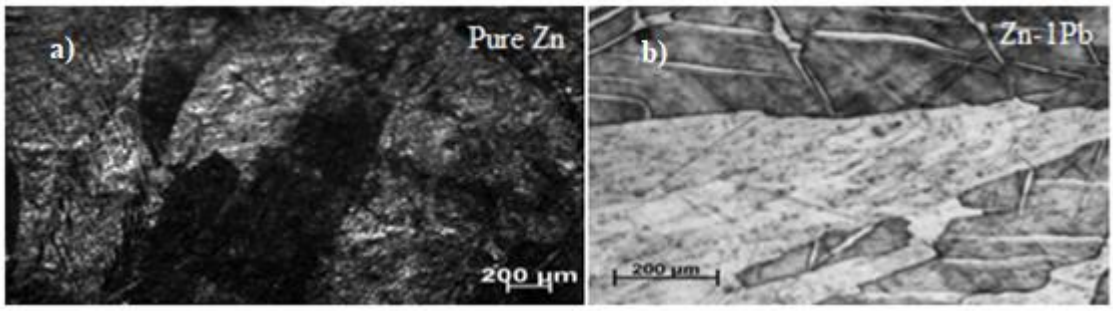

Fig.2. OM micrographs of, a) pure zinc and b) zinc-1 % wt. lead alloy after mechanical polishing and chemical attack in a solution (5ml of $HN0_3$ in 100 ml of deionized water) during 5 sec

However, when iron is present as an impurity in zinc at levels greater than 0.001%, it precipitates as an iron-zinc intermetallic compound called the ε phase containing about 6% iron. This phase is in the form of islands with a diameter between 0.5 and 30 µm [38]. Adding 1 % Pb to zinc changes its microstructure and causes evolution and degeneration of the eutectic. The lead-rich phase is in the form of small spherical particles of white colour distributed evenly in the zinc matrix. These small lead particles are torn off during polishing, due to their ductility, leaving behind them holes having the appearance of black spots in the microstructure [39,40]. Furthermore, porosity was observed in the structure of the Zn-1 % wt. Pb alloy [41].

2.3. Electrochemical measurements

2.3.1. Open Circuit Potential (OCP)

Passivation of pure Zn and Zn-1 % wt. Pb alloy was studied by following the variation of open circuit potential (OCP) in the same conditions, when samples were immersed in aerated 1.63 M H_2SO_4+ 0.9 M Zn^{2+} (pH 0.5 at 38°C) according to immersion time of 7 min. Each measurement started immediately after the working electrode was immersed in an acidic solution. These curves can monitor the chemical stability and reflect the initiation and propagation of dissolution [42]. After immersion a Zn oxide passive film began to grow on the surface of Zn electrode [43]. The potential resulting from the electrochemical reactions at the anode/solution interface was then recorded [44]. The relatively stable value was attributed to the slow and

regular reaction in the electrolyte [45]. For Zn-1 % wt. Pb alloy, the initial open circuit potential was around of -1008 mV/ SCE, rose slowly, but then gradually reaching a relatively stable value of -1002 mV /SCE after the time of passive film stabilisation of 365 s, this will enhance the free potential of the alloy. For unalloyed Zn, the initial potential is approximately -1004 mV/ SCE and the favour zinc deposition result in the shift of the potential towards the anodic direction [46-48]. This potential tends to become more noble with time stabilizing at-982mV/SCE after 312 s exposure. Lead had a very negative potential (-0.13 V/SHE) compared to that of zinc (-0.76 V/SHE), the measurement of the open circuit potential of Zn-1 % wt. Pb alloy showed that the lead addition led to a significant decrease in the free potential of this alloy, so it can be observed that the free potential of the Zn-1 % wt. Pb alloy showed more negative value with addition of lead. This alloy has the lowest potential value and the longest time to reach stable value, indicating its great tendency for dissolution.

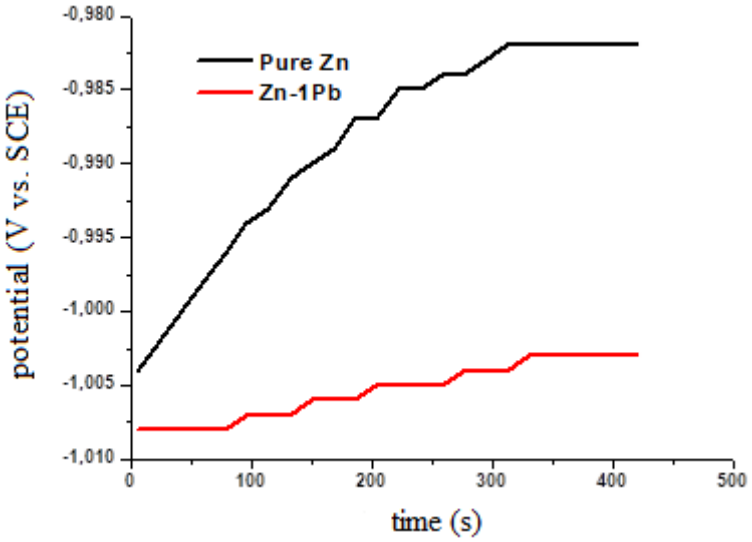

Fig.3. Evolution of the free potential for pure zinc and zinc-1 % wt. lead alloy in aerated 0.9 M $ZnSO_4.7H_20$ + 1.63 M H_2S0_4 at 38 °C

2.3.2. Potentiodynamic polarization curves

In Potentiodynamic polarization plots, the anodic polarization curve corresponds to the anodic dissolution of zinc and Zn-1 % wt. Pb alloy, while the cathodic polarization curve represents two possible reactions: the major zinc reduction reaction and the hydrogen evolution reaction through reduction of water. The hydrogen evolution reaction proceeds at significantly slower

rates, as compared to desired zinc reduction [49-51] The dissolution mechanism in zinc electrowinning electrolyte of 59 g.L^{-1} Zn^{2+} and 160 g.L^{-1} H_2SO_4 at 38 °C can be suggested as follows.

The anodic dissolution of Zn,

$$Zn \rightarrow Zn^{2+} + 2e^- \quad (1)$$

The main anodic reaction in sulfate electrolytes is the oxidation of water to oxygen

$$H_2O \rightarrow \frac{1}{2}O_2 + 2H^+ + 2e^- \quad (2)$$

Basic reaction

- Dissociated entities

$$ZnSO_4 \rightarrow Zn^{2+} + SO_4^{2-} \quad (3)$$

$$2H_2O \rightarrow 2H^+ + 2OH^- \quad (4)$$

- Reacting ions

$$Zn^{2+} + 2e^- \rightarrow Zn \quad (5)$$

$$2OH^- \rightarrow H_2O + \frac{1}{2}O_2 + 2e^- \quad (6)$$

$$SO_4^{2-} + 2H^+ \rightarrow H_2SO_4$$

At the cathode

$$Zn^{2+} + 2e^- \rightarrow Zn \quad (7)$$

$$2H^+ + 2e^- \rightarrow H_2 \quad (8)$$

- General reaction

$$Zn^{2+} + SO_4^{2-} + H_2O \rightarrow H_2SO_4 + Zn + \frac{1}{2}O_2 \quad (9)$$

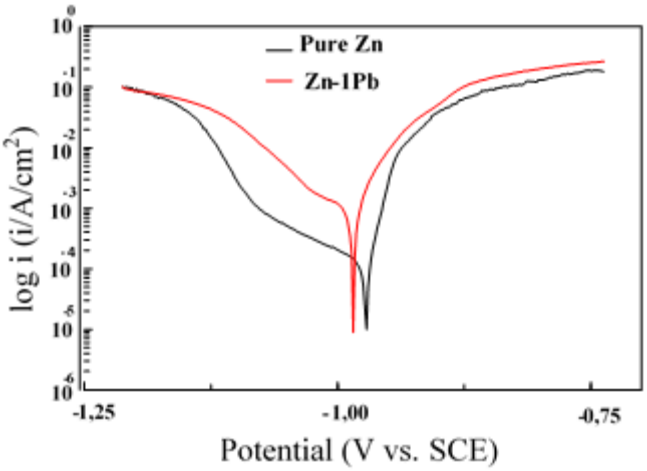

Fig.4. Polarisation curves of pure zinc and zinc-1 % wt. lead alloy in aerated 0.9 M $ZnSO_4.7H_20$ + 1.63 M H_2SO_4 at 38°C

As shown the figure 4, the cathodic polarization curve of pure Zn shows the little inflection point with two different slopes at potential value more negative than the corrosion potential, this is due to the effect of barrier formed by the deposition of the slime constructive by $ZnSO_4.7H_2O$, ZnO_2 and ZnO deposited on the surface of working electrode before and during immersion in the electrolyte [52]. The slime has a porous structure and consequently, the real passivation of Zn can't be reached [53].

Cathodic and anodic branches of the polarization curve of Zn-1 % wt. Pb alloy have shifted to higher current densities, compared with those of pure Zn. The dissolution process of Pb to Pb^{2+} ions in electrolyte is fast, accordingly lead exhibits low resistance in the acidic medium.

This indicates that the rate of hydrogen evolution and the anodic dissolution are fast. So, it is assumed that the presence of Pb as a minor alloying element increases the density of active sites on the surface.

Several kinetic parameters were determined from the extrapolation of Tafel curves. Results of corrosion current density (i_{corr}), corrosion potential (E_{corr}), anodic and cathodic slopes ($ß_a$ and $ß_c$) are obtained by the use of EGG.PAR M 352 Software and are summarised in table 2.

Table 2. Electrochemical parameters obtained from Tafel curves for pure zinc and zinc-1 % wt. lead alloy electrodes in aerated 0.9 M $ZnSO_4.7H_2O$ + 1.63 M H_2SO_4 at 38 °C

Samples	OCP (mV/SCE)	E_{corr} (mV/SCE)	i_{corr} (mA/cm^2)	Corr rate (mm/y)	$ß_c$ (mV/dec)	$ß_a$ (mV/dec)
Pure Zn	-982	-978.58	0.05781	0.8655	73.598	45.817
Zn-1Pb	-1002	-984.70	1.17770	17.6319	94.469	62.860

For pure Zn, The Tafel slopes ($ß_a$ and $ß_c$) are smaller than the Tafel slopes ($ß_a$ and $ß_c$) of the alloy Zn-1 % wt. Pb, these observations are correlated with the fact that the cathodic and the anodic exchange- current density values of the pure Zn are smaller than those of the alloy Zn-1 % wt. Pb. The corrosion potential E_{corr}, for pure Zn in absence of lead is more positive and reaches the value of -978.58 mV/ECS. This result was consistent with OCP-time curve measurements in figure 3. In the same time, pure Zn anode shows the lowest corrosion current density (0.05781 mA.cm^{-2}) and exhibits the best corrosion resistance among Zn-1 % wt. Pb alloy. So cathodic and anodic reactions are affected by the composition. The addition of 1% wt. Pb to Zn increases the corrosion rate 20.37 times indicating an increase in anodic dissolution.

2.3.3. Chronoamperometry

In order to accelerate the anodic process of dissolution of the zinc and its alloy and on the basis of the current-potential curve of figure 4, a potential of E_{corr} +10 mV vs saturated calomel electrode SCE, in the active zone was selected and applied to two electrodes pure Zn and Zn-1 % wt. Pb alloy at 38 °C for 3600. The behavior of dissolution for the two anodes was investigated by chronoamperometric curves reported in figure 5, enable to compare the activity of anodic dissolution during 1 hour. As shown in figure 5 the pure anode and the impure anode characterize the formation and the growth of a layer of sludge. The formation of sludge layer on the surface of the pure Zn causes a rapid decrease in current density and notice that its passivation is reached after 1630 s of polarization at E_{corr} +10 mV. The table 3 gives the characteristic parameters taken from the curve i-t of figure 5.

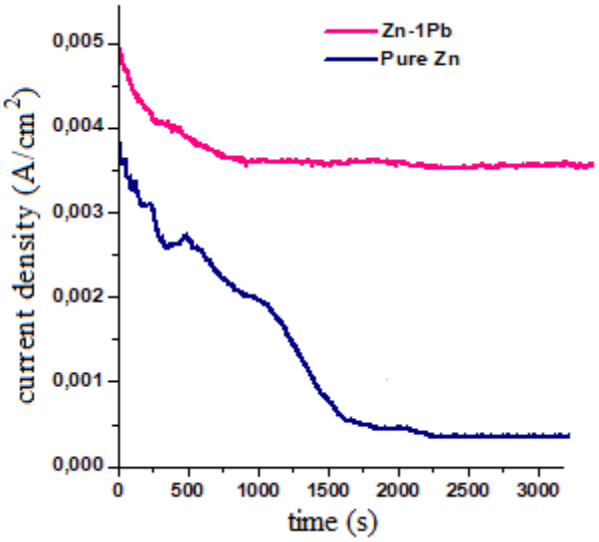

Fig.5. Chronoamperometric curves of two anodes of pure Zn and Zn-1 % wt. Pb alloy polarized at E = E_{corr} +10 mV during 1 h recorded in aerated solution of 0.9 M $ZnSO_4.7H_2O$ + 1.63 M H_2SO_4 at 38°C

Table 3. Characteristic parameters obtained from chronoamperometric curves of anodes of pure Zn and Zn-1 % wt. Pb alloy in aerated solution of 0.9 M $ZnSO_4.7H_2O$ + 1.63 M H_2SO_4 at 38°C

Anode	**i_{max} (mA/cm²)**	**i_{stab} (mA/cm²)**	**t_{stab} (seconds)**
Pure Zn	4.016	0.534	1630
Zn-1Pb	4.979	3.584	913

i-t curves show that at the beginning, a high current density is observed for two anodes, and it is followed by fast current decay which characterize the accumulation of the corrosive products and sludge formed on the active surface sites of two electrodes [54]. Stabilization time is characterised by very slow decrease in the current and correspond to the formation of the passive layer and its resistance. In the first 538 s, curve pure Zn presented the fluctuations, which can be interpreted as competitions between the initiation and ceasing in various areas. It is possible that corrosion stops in a corroded area but initiated in a new area [55]. i_{stab} gives information on the quality of the passivation film. As shown in table 3, the i_{stab} increased with

the lead impurity in the zinc anode. The current density of Zn-1 % wt. Pb alloy was higher than that of pure Zn at all the time, which confirm the high corrosion rate of Zn-1 % wt. Pb alloy and higher corrosion resistance of pure Zn [56]. The results of this part were in good agreement with Tafel results.

2.3.4. Electrochemical impedance measurements

Electrochemical impedance spectroscopy is a no destructive technique [53]. It has been applied for characterisation of the dissolution and the passivation of metals [14]. In order to describe the evolution of impedance, selective impedance spectra at different immersion times have been analysed using ZView 2 software. Impedance spectrums in the representation of Nyquist and Bode plots recorded during five hours of immersion in the solution of 0.9 M $ZnSO_4.7H_2O$ + 1.63 M H_2SO_4 at 38℃ are shown in figure 6 for the pure Zn and in figure 7 for Zn-1 % wt. Pb alloy. The measurements were performed by applying an AC amplitude of 10 mV in the frequency range comprised from 100 KHz to 10 mHz at open circuit potential [57].

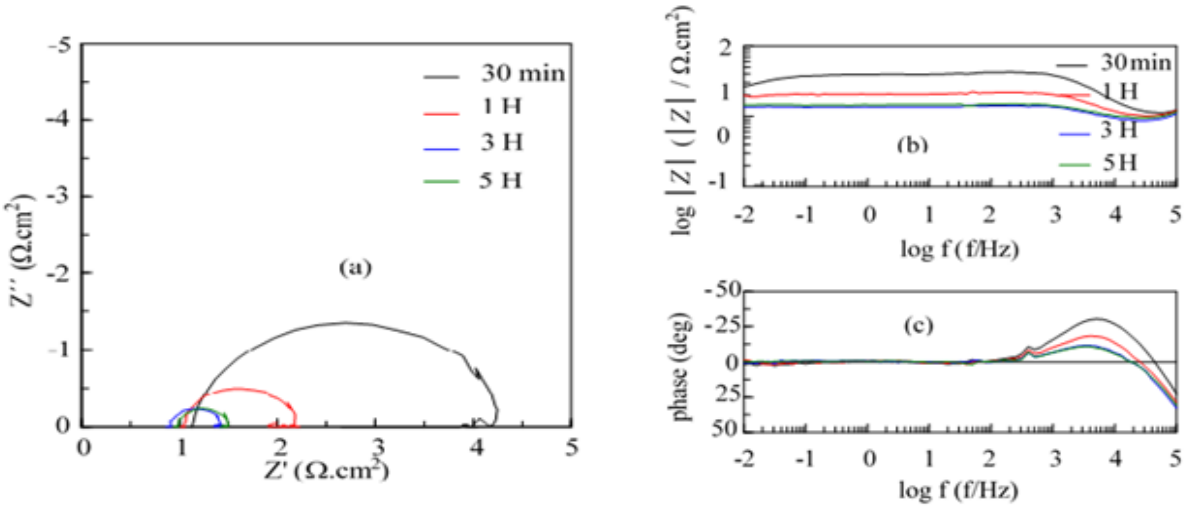

Fig.6. Electrochemical impedance spectroscopy diagrams of pure Zn at OCP in aerated solution of 0.9 M $ZnSO_4.7H_2O$ + 1.63 M H_2SO_4 at 38 °C, (a) Nyquist plots (b) Bode magnitude

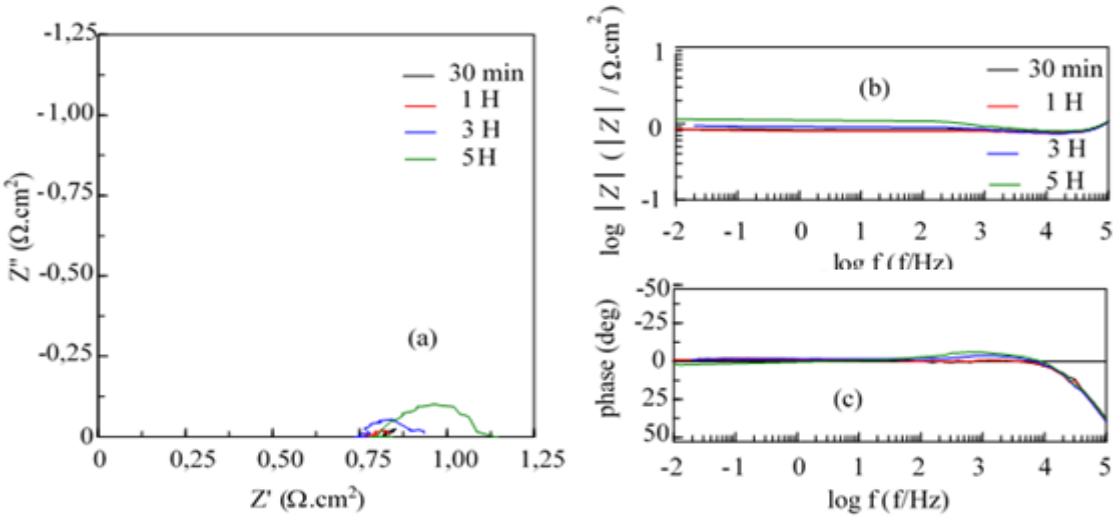

plots (c) Bode phase plots.

Fig.7. Electrochemical impedance spectroscopy diagrams of Zn-1 % wt. Pb alloy at OCP in aerated solution of 0.9 M $ZnSO_4.7H_2O$ + 1.63 M H_2SO_4 at 38 °C, (a) Nyquist plots (b) Bode magnitude plots (c) Bode phase plots

The quantitative analysis was made by fitting the data using equivalent circuit model presented in figure 8 as model for the corrosion system on basis of the literature [56-62]. The fitted results are shown in Table 4 In the equivalent circuit, R_s represents the solution resistance between the reference electrode (RE) and working electrode (WE), R_{ct} and C_{dl} represents the charge transfer resistance, in parallel to the double-layer capacitance of electrode/electrolyte interface.

Fig.8. Equivalent circuit of two interfaces: pure Zn and Zn-1 % wt. Pb alloy / aerated solution (0.9 M $ZnSO_4.7H_2O$ + 1.63 M H_2SO_4) at OCP and at 38 °C

Table 4. Electrochemical impedance parameters obtained for pure Zn and Zn-1 % wt. Pb alloy as a function of immersion time at OCP in aerated solution of 0.9M $ZnSO_4.7H_20$ + 1.63M H_2S0_4 at 38 °C

Material	**Immersion time (h)**	**R_s ($\Omega.cm^2$)**	**C_{dl} ($\mu F/cm$)**	**R_{ct} ($\Omega.cm^2$)**
Pure Zn	1/2	1.256	20.943	2.902
	1	1.098	55.462	1.063
	3	0.931	120.760	0.483
	5	1.167	103.900	0.542
Zn-1Pb	1/2	0.855	3146.000	0.028
	1	0.772	4921.200	0.024
	3	0.773	1267.500	0.123
	5	0.838	984.050	0.216

Table 4 shows the fitted electrochemical impedance parameters of pure Zn and its alloy at OCP. The best fitting equivalent electrical circuit is realized with relative error less than 10 %. The calculation of the kinetic and electrical parameters of RC circuit is a simple way of understanding the medium effect on the anodic dissolution of zinc.

It can be observed that there is one perfect semicircle on both complex plane plots for each sample which means that the passive films are compacts [63]. The semi diameter is directly related to the property of corrosion resistance (R_p), a bigger semi diameter represents a better corrosion resistance property of the electrode. C_p values are extracted by using equation (10) to the frequency at the maximum of the semicircle.

$$\omega_{max}.R_p.C_p = 1 \quad (10)$$

The Niquist plots exhibited only one complex capacitive loop at high frequency range, and the Bode plots suggest one time constant well distinguished between 100 KHz and 10 mHz. This time constant at high frequencies (R_{ct} and C_{dl}) is attributed to the charge transfer layer, and is relative to properties of the corrosion product layer [23,64]. Theoretically, corrosion rate is

inversely proportional to the polarization resistance, which may be related to the processes of charge transfer and protective films.

According to figure 6, R_{ct} of pure Zn keep decreasing as the immersion time increases revealing that the corrosion resistance of pure Zn degrades with time. This may be ascribed to the gradual destruction of the film. After 3 h of immersion, the shape of impedance diagram become practically independent of time and the value of transfer resistance become nearly constant. The double layer capacitance was also unchanged. One can assume that in this case, an equilibrium between the dissolution of the material and the development of the protective layer is reached. Such impedance spectra appear in materials exposed to aggressive media when they become severely corroded. This evolution of impedance is revealed in the Bode plots as an important decrease of the phase angle and impedance modulus with the immersion time due to the damage of the barrier as shown in figure 6. It is clear that phase angle maxima corresponding to pure Zn is large at high frequency compared to the alloy and its impedance modulus at a low frequency, lZl value is the highest which is an indication of a good barrier protection because Zomorodian and al [65,66] reported that the low frequency modulus could be used as an indicator of the coating protective effect. At low frequency, frequencies are independent of phase angle. It will be noted for Zn-1 % wt. Pb alloy in figure 7 (b) that the band is quite narrow except at the lowest frequencies.

With prolonged electrolysis, table 4 lists parameters deducted from EIS spectrums, the R_s values of two samples are similar because the electrolyte is the same. For pure Zn the charge-transfer resistance R_{ct} decreases, whereas C_{dl} increases. On the other hand, for Zn-1 % wt. Pb alloy the charge transfer resistance decreases until 1 h, after which it increases, at the same time the capacity increases until 1 hour after it decreases. Pure Zn has a high value resistance (2.902 $\Omega.cm^2$) and low value capacitance (20.943 μF/cm) therefore pure Zn had a better comprehensive protection than Zn-1Pb alloy. Lead addition decreased the charge transfer resistance further and increased the double layer capacitance, which can be used as an indicator for the change of the passive film thickness [43,67].

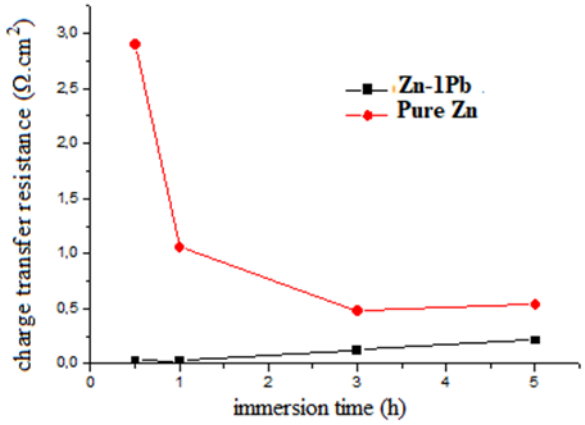

Fig.9. Charge transfer resistance R_{ct} of pure Zn and Zn-1Pb alloy at different immersion time in aerated solution of 0.9 M $ZnSO_4.7H_2O$ +1.63 M H_2SO_4 at T=38 °C

From the curves of the figure 9, the charge transfer resistance is a function of immersion time, figure 9 shows that the resistance of pure Zn decreases in two distinct periods. Firstly, between 1/2 and 1 hour, the R_{ct} decreases due to the rapid degradation of the layer. Secondly, between 1 and 3 hours, the R_{ct} loses about 1/2 factor of its second value then tends to level off. Such stabilization may be due to build-up of stable layer of slime products [68].

Comparing with Zn-1 % wt. Pb alloy, the values of R_{ct} of pure Zn is larger during the entire immersion indicating that pure Zn without lead addition is conductive to form a higher thickness, more homogenous and compact slime product layer [63,69-71]. Zn-1 % wt. Pb alloy exhibit lower R_{ct} in the same time of immersion, this implies that the film formed on Zn-1Pb alloy is less compact and less resistant than that formed with pure Zn. The presence of 1% of lead in the alloy can change the dissolution behavior of pure zinc. Pb^{2+} may penetrate the passive film on zinc surface or incorporate in the film as an impurity, thus altering its physical and electrical properties. As a result, lead ions (Pb^{2+}) will lead to breakdown the passive film and active dissolution at many local sites on zinc surface. Pb addition plays the important role in increasing the dissolution rate of the alloy in the acidic solution.

The results of the R_{ct} confirm for the two anodes the same trend by Tafel results (Tables 2 and 4). Indeed, we note that R_{ct} for pure zinc is high (between 0.483-2.902 $\Omega.cm^2$), which is consistent with the lowest value of i_{corr} (0.057 mA/cm^2) of the same R_{ct} for Zn-1Pb alloy is

low (between 0.024-0.216 Ω.cm^2), which is consistent with the high value of i_{corr} (1.177 mA/cm^2).

The absence of Pb in Zn was found to refine the effective grain size, consequently, to improving the barrier performance. By correlating the two microstructures in figure 2 with the corresponding EIS results, it is also possible to observe a trend for better dissolution resistance related to more refined sample [53,72].

3. EXPERIMENTAL METHODS

The electrochemical properties of pure Zn and Zn-1 % wt. Pb alloy were studied in acidic sulfate electrolyte at T=38°C and were measured by quasi-stationary Tafel polarization, chronoamperometry and electrochemical impedance spectroscopy (EIS) in order to evaluate the electrochemical performance, the passivation and the activation of these two anodes.

3.1. Preparation of electrodes

Electrodes from pure zinc (purity of 99.79%, METANOF, El Ghazaouat, Algeria) and Zn-1 % wt. Pb alloy (Pb purity of 99.99%), were melted in carbur silicium crucibles using a muffle furnace (type CONTROLABO**)** heated under a speed of 5°C/min up to 500°C, under Argon flow (to prevent oxidation) and under a pressure of 10^{-2} bar.

The cast alloys were cooled down in air on graphite crucibles. The cylinders obtained of 6 cm in length and 1.36 cm² of surface area were transversely cut with a laboratory saw (type BROT) into small cylinders of 1 cm length, connected to a copper wire isolated with plastic and cast in transparent (Araldite cy 230 and 10% of hardner hy 951) with an exposed area of 1.36 cm². All working surfaces of the anodes and cathodes were mechanically polished under water with SiC abrasive paper from 180, 600, 800 to 1200 grit. The obtained mirror-smooth surface must be ultrasonically washed, degreased in acetone to eliminate dirt on the surface of the electrodes, rinsed with bidistilled water and finally dried by hot air (compressed air). After that, the electrode was immediately transferred into the electrochemical cell.

3.2. Electrochemical cell and electrolyte

The working electrodes were pure Zn and Zn-1 % wt. Pb alloy cylinder of 1.36 cm in diameter. The auxiliary electrode is pure Zn cylinder of 2 cm in diameter, the two electrodes were

mounted in Bakelite sample port fixed to the lid of a 1000 cc beaked cell by plastic bats. The distance separating the anode from cathode was 22 mm. $Hg/Hg_2Cl_2/Cl^-$ (0.24V (vs NHE)) a saturated calomel electrode (SCE) was employed as the reference electrode.

Experiment was carried in naturally aerated while the zinc electrolyte used in electrolysis was prepared from analytical sulphuric acid (98%), salt zinc sulphate $ZnSO_4.7H_2O$, and bidistilled water. This electrolyte had 6g/L (=1.63 M) H_2SO_4 + 60 g/L (=0.9 M) Zn^{2+}which was the same as the industrial electrowinning electrolyte. The temperature of the solution was controlled at (38 ± 0.2) °C by a thermostatic water bath (LAUDA) and the pH value measured was about 0.5.

3.3. Experimental measurements

3.3.1. chemical analysis

The analysis was carried out directly on the sample which was cut into a cylindrical shape of 3 cm in diameter and 0.5 cm in thickness, the sample surface undergoes a high polishing. This analysis has been carried out using a spectrometer (Bruker-Axs: SRS3400) equipped with X ray tube with rhodium anode. Data was processed by software (Spectra 3000 AT). The concentration of an unknown sample was determined by the calibration curves that are plotted for each element after setting the measurement parameters (kV-mA, crystal analyser, collimator, emission wavelength, measurement time and detector).

3.3.2 Surfaces characterization

The microstructure of pure Zn and its alloy were examined first by metallographic optic microscope (OM) (Zeiss, AXIOTECH HAL 100, AXIO CAM MRC 5). Samples for OM were polished by a standard metallographic procedure and etched in a solution (5 ml of HNO_3 in 100 ml of deionized water) during 5 seconds, rinsed with ethanol then dried with hot air (compressed air). The diffractograms of samples were obtained using the conventional X-ray diffractometer (XRD, PANALYTICAL: XPERT-PRO) using CuKα monochromatic radiation (λ= 1.5418 Å) with an acceleration voltage of 45 kV and a filament current of 40 mA at 298 K with the angle range of 2Ɵ=2 to 70 degree (scan step size 0.0170°, time per step 87.2256 s and scan type was continuous). The diffraction patterns were recorded for the identification of constituent phases of Zn and its alloy Zn-1 % wt. Pb.

3.3.3. Electrochemical measurements

The corrosion properties of all samples were evaluated by Tafel Potentiodynamic polarisation, chronoamperometry and EIS techniques.

A Princeton Applied Research Potentiostat-Galvanostat EG & G PARC model 273 A (Speed Control Unit CTV 101 Radiometer Analytical, Shlumberger SI 1260 Impedance Gain-Phase Analyser) was used to apply perturbation and to acquire the response. The measurements were controlled by an HP BRIO computer.

Prior to the electrochemical measurement, the working electrode was maintained at free potential during 7 minutes and the open-circuit (OCP) was monitored. All measured potentials were reported versus the SCE reference electrode. After wards, Potentiodynamic polarisation curves were recorded at a potential scan rate of 1.016 mV/s. Corrosion parameters including corrosion potential (E_{corr}) and corrosion current density (i_{corr}) were recorded from Tafel plots, analysed by auto fitting. The formation and evolution of dissolution and slime forming on pure Zn and Zn-1% wt. Pb anodes during Potentiostatic control was realised by applying a constant potential ($E_{corr+10mV}$). After 2000 s of anodic control, polarisation curves were recorded. During EIS measurement, an AC amplitude of 10 mV was applied, at the free potential. The impedance spectra were recorded in the frequency range from 100 kHz to 10 mHz. Impedance data were recorded by the use of the ZView software of Solartron, the same software was used to select the equivalent electrical circuits.

An equivalent circuit model was proposed to characterize Zn/slime and slime/solution electrochemical interface. The electrochemical behaviour of the anode during the zinc electro-refining is very important for the anodic reactions as well as for the quality of zinc deposit.

4. CONCLUSIONS

In zinc electrorefining process, the effect of minor lead (Pb) alloying with zinc on the anode dissolution of zinc in aerated acidic zinc sulphate solution at 38 °C was investigated by different techniques. Based on the results above, the conclusion can be summarised as follows:

- ✓ Pure zinc and Zn-1 % wt. Pb alloy anodes were characterized using XRD. The addition of 1% to lead changed as cast microstructure.
- ✓ Passivation of pure Zn and its alloy was studied by following the variation of open circuit potential (OCP). The Zn-1 % wt. Pb alloy has the lowest potential value and the longest time to reach stable value indicating its big tendency to dissolution.
- ✓ The data of Tafel plot showed that the cathodic and anodic branches shift to higher current densities on the alloy surface compared with those of pure zinc. Positive shift in corrosion potential (E_{corr}) with simultaneous increase in the dissolution rate of the alloy compared with the pure zinc are obtained. This indicates that the presence of impurity of Pb increase the anodic dissolution current of the alloy, and improves its instability against activity.
- ✓ Potentiostatic measurements reveal that, the current density decreases with the increase of time. This may be attributed to the formation of thick barrier layer at applied potential (E_{cor}+10mV).
- ✓ The EIS results, very well fitted using a simplified Randles standard equivalent circuit model (R_s (C_{dl} R_{ct})), assumes that the charge transfer resistance (R_{ct}) is lower and the capacity of the double layer (C_{dl}) value is higher for Zn-1 % wt. Pb alloy compared with those of pure zinc during 5 hours of immersion. This behaviour is in good agreement with that obtained from Tafel plot and potentiostatic measurements.
- ✓ Taking into account the previous points, it is confirmed that the addition of lead to the zinc anode as an impurity accelerates its degradation.

5. ACKNOWLEDGEMENTS

Authors thank CRD-Sonatrach of Boumerdes, for electrochemical tests (Corrosion Laboratory), X-RD and SEM morphology. Writers are grateful to Metallurgy Laboratory for zinc alloys elaboration.

6. REFERENCES

[1] Darcy. M. Métallurgie du zinc. Techniques de l'ingénieur. M 2270, 1974.

[2] Yang. H.T, Guo. Z.C, Chen. B.M, Liu. H.R, et al. Electrochemical behavior of rolled Pb-0.8 % Ag anodes in acidic zinc sulfate electrolyte solution containing Cl-ions. Hydrometallurgy. (2014) 147, 148-156.

[3] Sole. K.C. The influence and benefits of an upstream solvent-extraction circuit on the electrowinning of zinc in sulfate media. Research Gate. (2016), 1-9.

[4] Zhou. X, Wang. S, Yang. J, et al. Effect of cooling ways on properties of Al / Pb-0.2 % Ag rolled alloy for zinc electrowinning. Trans. Non ferrous Met. Soc. China. (2017) 27, 2096-2103.

[5] Diban. N, Mediavilla. R, Urtiaga. A, et al. Zinc recovery and waste sludge minimization from chromium passivation baths. Journal Hazardous Materials. (2011), 192, 801-807.

[6] Chen. Y, Yech. H, Lo. N, et al. Electrodeposition of compact zinc from the hydrophobic brØnsted acidic ionic liquid-based electrolytes and the study of zinc stability along with the acidity manipulation. Electrochimica Acta,
doi: https://doi.org/10.1016/j.electacta.2017.01.013

[7] Ma. H.W, Matsubae. K, Nakajima. K, et al. Substance flow analysis of zinc cycle and current status of electric furnace dust management for zinc recovery in Taiwan. Resour. Conserv. Recycl. (2011) 56, 134-140.

[8] Abkhoshk. E, Jorjani. E, Al Harahsheh. M.S, et al. Review of the hydrometallurgical processing of non-sulfide zinc ores. Hydrometallurgy. (2014) 149, 153-167.

[9] Nady. H. Tricine [N- (Tri (hydroxymethyl) methyl) glycine] - A novel green inhibitor for the corrosion inhibition of zinc in neutral aerated sodium chloride solution. Egyptian Journal of Petroleum. (2016), 1-9.

[10] Bakkar. A, Neubert. V. Recycling of cupola furnace dust: Extraction and electrodeposition of zinc in deep eutectic solvents. Journal of alloys and compounds. (2018). doi:https://doi.org/10.1016/j. jallcom.2018.08.246

[11] Luo. J.Z.P, Duan. N, Jiang. L, et al. Interpretation of material flow analysis results and a case study on cleaner production for waste water source reduction in a zinc electrolysis cellhouse. Journal of Cleaner Production. (2018). doi: 10.1016/j. jclepro.2018.01.146.

[12] Qi. C, Ye. L, Max, et al. Life cycle assessment of the hydrometallurgical zinc production chain in China. Journal of Cleaner Production. (2017).
doi: https://doi.org/10.1016/j. jclepro.2017.04.084

[13] Ares. A.E, Gassa. L.M. Corrosion susceptibility of Zn-Al alloys with different grains and dendritic microstructures in NaCl solutions. Corrosion Science. (2012) 59, 290-306.

[14] Giménez-Romero. D, García-Jareño. J.J, Vicente. F. Analysis of an impedance function of zinc anodic dissolution. Journal Electroanalytical Chemistry. (2004) 57, 235-247.

[15] Jha. M.K, Kumar. V, Singh. R.J. Review of hydrometallurgical recovery of zinc from industrial wastes, Resources. Conservation and Recycling. (2001) 33, 1-22.

[16] Xueyi. G, Yuga. Z, Yu. S. Substance flow analysis in China. Resources. Conservation and Recycling. (2010) 54, 171-177.

[17] Et Taouil. A, Mahmoud. M.M, Lallemand. F, et al. Corrosion protection by Sonoelectrodeposited organic films on zinc coated steel. Ultrasonics Sonochemistry. (2012) 19, 1186-1193.

[18] Huajun. Z, Zhenghai. G, Yunpeng. Z. Electrorefining zinc dross in ammoniacal ammonium chloride system. Hudrometallurgy. (2008) 90, 8-12.

[19] Yang. C.J, Park. S. Electrochemical behaviour of PbO2 nanowires array anodes in a zinc electrowinning solution. Electrochimica Acta. (2013) 86-94.

[20] Taguchi. M, Takahashi. H, Nagai. M, et al. Chracteristics of Pb-based alloy prepared by powder rolling method as an insoluble anode for zinc electrowinning. Hydrometallurgy. (2013) 136, 78-84.

[21] Herraiz-Cardona. I, Ortega. E, Pérez-Herranz. V. Evaluation of the Zn^{2+} transport properties through a cation-exchange membrane by chronopotentiometry. Journal of Colloid and Interface Science. (2010) 341, 380-385.

[22] Herrevo. D, Arias. P.L, Güemez. B, et al. Hydrometallurgical process development for the production of a zinc sulphate liquor suitable for electrowinning. Minerals Engineering. (2010) 23, 511-517.

[23] Kaewmaneekul. T, Lothongkum. G. Effect of aluminium on the passivation of zinc-aluminium alloys in artifitial seawater at 80°C. Corrosion Science. (2013) 66, 67-77.

[24] Möller. C.A, Friedrich. B. effect of As, Sb, Bi and oxygen in copper anodes during electrorefinin. IME Process Metallurgy and Metal Recycling. (2010) 1495-1510.

[25] Rimaszeki. G, Kulcsar. T, Kekesi. T. Application of HCl solutions for recovering the high purity metal from tin scrap by electrorefining. Hydrometallurgy. (2012) 125-126, 55-63.

[26] Jafari. S, Kiviluoma. M, Kalliomäki. T, et al. Effect of typical impurities from the formation of floating slimes in copper electrorefining. Minpro. (2017). doi: 10.1016/j.minpro.2017.09.016.

[27] Larouche. P. Minor elements in copper smelting and electrorefining. Thesis. Nov (2001) Canada.

[28] Ojaghi Ilkhchi. M, Yoozbashizadeh. H, Sadegh Safarzadeh. M. The effect of additives on anode passivation in electrorefining of copper. Chemical Engineering and Processing. (2007) 46, 757-763.

[29] Liu. L, Tan. J, Liu. X. Reactive brazing of Al alloy to Mg alloy using zinc-based brazing alloy. Materials Letters. (2007) 61, 2373-2377.

[30] Ren. X, Wei. Q, Hu. S, et al. The recovery of zinc from hot galvanizing slag in an anion-exchange membrane electrolysis reactor. Journal of Hazardous Materials. (2010) 181, 908-915.

[31] Guessoum. K, Veys-Renaux. D, Rocca. E, et al. Corrosion behavior of zinc-cerium alloys: Role of intermetallic phases. Corrosion Science. (2011) 53, 1639-1645.

[32] Noor. F, Wen. D. Experimental study of thermal oxidation of nanoscale alloys of aluminium and zinc (nAlZn). Journal of physics and chemistry of solids. (2015) 85,188-196.

[33] Ma. R, Cheng. S, Zhang. X, et al. Oxygen evolution and corrosion behavior of low -MnO2-content Pb-MnO2 composite anodes for metal electrowinning. Hydrometallurgy. (2016) 159, 6-11.

[34] Liu. Z, Li. R, Jiang. R, et al. Effects of Al addition on the structure and mechanical properties of Zn alloys. Journal of Alloys and Compounds. (2016) 687, 885-892.

[35] Mathabatha. M.H, Popoola. A.P.I, Oladijo. O.P. Residual stresses and corrosion performance of plasma sprayed zinc-based alloy coating on mild steel substrate. Surface & Coatings Technology. (2016).

[36] Safizadeh. F, Su. C, Ghali. E, Houlachi. G. The effect of lead and some operating parameters on cathode contamination during zinc electrowinning. Hydrometallurgy. (2017) 171, 69-76.

[37] Alesary. H.F, Cihangir. S, Ballantyne. A.D. Influence of additives on the electrodeposition of zinc from a deep eutectic solven. Electrochimica Acta. (2019).
doi: https://doi.org/10.1016/j.electacta.2019.02.090

[38] Mera. M.F, Rubio. M, Pérez. C.A, et al. SRμXRF and XRD study of the spatial distribution and mineralogical composition of Pb and Sb species in weathering crust of corroded bullets of hunting fields. Microchemical Journal. (2015) 119, 114-122.

[39] El-Sayed. A., Mohran. H.S, Abdel Shafy Shilkamy. H. Effect of phosphoric acid concentration on conductivity of anodic passive film formed on surface of lead-indium alloy. Trans. Nonferrous Met. Soc. China. (2016) 26, 882-894.

[40] Kim. E, Horckmans. L, Spooren. J, et al. Selective leaching of Pb, Cu, Ni and Zn from secondary lead smelting residues. HYDROM. (2017), pp. 4533.

[41] wang. Y, Kong. G, Che. C. Corrosion behavior of Zn-Al alloys in saturated Ca $(OH)_2$ solution. Corrosion Science. (2016) 112, 679-686.

[42] Roche. M. Protection contre la corrosion des ouvrages maritimes pétroliers. Tome 1, premier fascicule I.E.P. France, 1978.

[43] ASM International. Metallography and microstructures of zinc and its alloys. ASM Handbook. (2004) 9, 933-941.

[44] Valdez. S, Genesca. J, Mena. B, et al. Journal of Materials Engineering and Performance. (2001) 10(5), 596-601.

[45] Van den Bos. C, Schnitger. H.C, Zhang. X, et al. Influence of alloying elements on the corrosion resistance of rolled zinc sheet. Corrosion Science. (2006) 48, 1483-1499.

[46] Wang. N, Wang. R, Peng. C, et al. Corrosion behavior of Mg-Al-Pb and Mg-Al-Pb-Zn-Mn alloys in 3.5 % NaCl solution. Trans. Nonferrous Met. Soc. China. (2010) 20, 1936-1943.

[47] Zohdy. K.M, Sadawy. M.M, Ghane. M. Corrosion behavior of leaded-bronze alloys in sea water. Materials Chemistry and Physics. (2014) 147, 878-883.

[48] Zhang. W, Robichaud. M, Ghali. E, et al. Electrochemical behavior of mesh and plate oxide coated anodes during zinc electrowinning. Trans. Nonferrous Met. Soc. China. (2016) 36, 589-598.

[49] Li. J, He. X, Hang. R, et al. Fabrication and corrosion behavior of TiO2 nanotubes on AZ91D magnesium alloy. Ceramics International. (2017) Ref CERI 15799.

[50] Bounoughaz. M, Salhi. E, Benzine. K, Ghali. E, et al. A comparative study of the sacrificial anode. Journal of Materials Science. (2003) Volume 38N6, 1339-1445.

[51] Jegannathan. S, Saukara Narayanan. T.S.N, Ravichandran. K, et al. Performance of zinc phosphate coatings obtained by cathodic electrochemical treatment in accelerated corrosion tests. Electrochimica Acta. (2005) 51, 247-256.

[52] Rosalbino. F, Scavino. G, D Maccíò. D, et al. Influence of the alloying component on the corrosion behaviour of zinc in neutral aerated sodium chloride solution. Corrosion Science. (2014), 00436-3.

[53] Havery J.F, D. Paul S. Synthesis, matching and deconstruction of polarization curves for the active corrosion of zinc in aerated near-nentral NaCl solutions. [J]. Corrosion Science. (2010) 52, 1905-1914.

[54] Badawy. W.A, Nady. H, Abd El-Hafez. G.M. Electrodeposited Zn-Ni alloys as promising catalysis for hydrogen production-preparation, characterization and electro-catalytic activity. Journal of Alloys and Compounds. (2017).

doi: https://doi.org/10.1016 / j. jallcom. 2016.12.228

[55] Abd El-Lateef. H.M, El-Sayed. A, Mohran. H.S. Role of nickel alloying on anodic dissolution behaviour of zinc in 3.5% NaCl solution. Part II: Potentiodynamic, potentiostatic and galvanostatic studies. Trans. Nonferrous Met. Soc. China. (2015) 25, 3152-3164.

[56] Lee. M, Kim. Y, Lim. K, et al. Electrochemical evaluation of zinc and magnesium alloy coatings deposited on electrogalvanized steel by PVD. Trans. Nonferrous Met. Soc. China. (2013) 23, 876-880.

[57] El-Sayed. A, Mohran. H.S, Abd El-Lateef. H.M. Effect of minor nickel alloying with zinc on the electrochemical and corrosion behavior of zinc in alkaline solution. Journal of Power Sources. (2010) 195, 6924-6936.

[58] Kehar. S. and Ragësh Kumar. P. Electrosynthesis and impedance studies on zinc selenide. Electrochimica Acta. (1994) Vol 39, N°18, 2693-2697.

[59] Nogueira Grosser. F, Gonçalves. R.S. Electrochemical evidence of caffeine adsorption on zinc surface in ethanol. Corrosion Science. (2008) 50, 2934-2938.

[60] Kellou-Kerkouche. F, Benchettara. A, Amara. S. Effect of sodium dodecyl benzene sulfonate on the corrosion inhibition of Fe-1Ti-20C alloy in 0.5 M H_2SO_4. Materials Chemistry and Physics. (2008) 110, 26-33.

[61] Yang. C.J, Ko. Y, Park. S. Fourier transform electrochemical impedance spectroscopic studies on anodic reaction of lead. Electrochimica Acta. (2012) 78, 615-622.

[62] Shi. C, Shao. Y, Wang. Y, et al. Influence of submicron-sheet zinc phosphate synthesised by sol-gel method on anticorrosion of epoxy coating. Progress in Organic Coatings. (2018) 117, 102-117.

[63] Yang. C, Zhang. Z, Tian. Z, et al. Influences of carboxymethyl cellulose on two anodised-layer structures of zinc in alkaline solution. Journal of Alloys and Compounds. (2018) 734, 152-162.

[64] Bakhsheshi-Rad. H.R, Hamzah. E, Ismail. A.F, et al. In vitro degradation behaviour, antibacterial activity and cytotoxicity of TiO2-MAO/Zn HA composite coating on Mg alloy for orthopaedic implants. Sct (2017). doi: https://doi.org/10,1016/j. surfcoat. 2017.11.027

[65] Zomorodian. A, Garcia. M.P, Silva. T.M, et al. Biofunctional composite coating architectures based on polycaprolactone and nanohydroxyapatite for controlled corrosion activity and enhanced biocompatibility of magnesium AZ31 allo. Mater. Sci. Eng. C. (2015) 48, 434-443.

[66] Liu. Y, Zhou. X, B. Stuart, et al. An organic coating pigmented with strontium aluminium polyphosphate for corrosion protection of zinc alloy coated steel. Progress in Organic Coatings. (2016).

[67] Zhang. P, Ó Keefe. T.J, Yu. P. Electrochemical characterization of the effects of impurities and organic additives in lead electrowinning from fluoborate electrolyte. Hydrometallurgy. (2001) 61, 207-221.

[68] Hamlaoui. Y, Pedraza. F, Tifouti. L. Corrosion monitoring of galvanised coatings through electrochemical impedance spectroscopy. Corrosion Science. (2008) 50, 1558-1566.

[69] Gu. X.N, Zheng. W, Cheng. Y, et al. A study on alkaline heat-treated Mg-Ca alloy for the control of the biocorrosion rat. Acta Biomater. (2009) 5, 2790-2799.

[70] Montemor. M.F. Functional and smart coatings for corrosion protection: A review of recent advances. Surf. Coat. Technol. (2014) 258, 17-37.

[71] Sankara Narayanan. T.S.N, Park. S, Lee. M.H. Strategies to improve the corrosion resistance of microarc oxidation (MAO) coated magnesium alloys for degradable implants: Prospects and challenges. Prog. Mater. Sci. (2014) 60, 1-71.

[72] Vida. T.A, Conde. A, Freitas. E.S. Directionally solidified dilute Zn-Mg alloys: Correlation between microstructure and corrosion properties. Journal of Alloys and Compounds. (2017) 723, 536-547.